periodica polytechnica

Mechanical Engineering
55/1 (2011) 29–37
doi: 10.3311/pp.me.2011-1.04
web: http://www.pp.bme.hu/me

RESEARCH ARTICLE

Modelling of metal matrix syntactic foams – Description of the compressive stress-strain curves

Eymeric de Lorgeril / *Frédéric* Wyss / *Imre Norbert* Orbulov

Received 2011-04-30

Abstract

This paper deals with the mathematical description of metal matrix syntactic foams (MMSFs). MMSFs are advanced materials having promising application fields in aviation, transport and automotive industry, in civil engineering and in many other industrial fields. They are porous materials having low density and relatively high compression strength especial compared to 'conventional' metallic foams. The characterization of MMSFs is continuously developing but the mathematical description of the compressive stress – strain curves is still missing partially. However these formulas are needed to numerically model the non-linear response and energy absorption of the MMSFs in case of compressive loading. According to this the aim of this paper is to give a full, but relatively simple method to handle the compressive stress – strain curves.

Keywords

syntactic foam · metallic foam · metal matrix composite · upsetting test · modelling.

Acknowledgement

The Metal Matrix Composites Laboratory is supported by Grant # GVOP 3.2.1-2004-04-0145/3.0. This paper was supported by the János Bolyai Research Scholarship of the Hungarian Academy of Sciences. The investigations were supported by The Hungarian Research Fund, NKTH-OTKA PD 83687. This work is connected to the scientific program of the " Development of quality-oriented and harmonized R+D+I strategy and functional model at BME" project. This project is supported by the New Széchenyi Plan (Project ID: TÁMOP-4.2.1/B-09/1/KMR-2010-0002). Thanks to R. Tóth and C. H. Erbslöh Hungaria Ltd. for providing E-spheres.

Eymeric de Lorgeril
Frédéric Wyss
Ecole Nationale Supérieure de Techniques Avancées ParisTech„ 32 Boulevard Victor Paris 15, French

Imre Norbert Orbulov
Department of Materials Science and Engineering, BME, H-1111, Budapest,Bertalan Lajos street 7, Hungary

1 Introduction

Metal matrix syntactic foams (MMSFs) are metal matrix composites consisting of a metallic matrix and ceramic hollow microballoons. Due to the hollow microballoons they can be also considered as porous materials or as metallic foams. The most common matrix materials are aluminium alloys (namely Al99.5 and AlSi12, but other alloys are also popular). The ceramic microballoons are composition of various oxide ceramics. They contain ∼35-40 wt% Al_2O_3 and ∼55-60 wt% SiO_2. MMSFs have low weight, outstanding specific properties, localized failure, good creep resistance, etc. The specific mechanical properties of MMSFs can be 50-100% higher than the "conventional" foams' [1, 2]. They are used as energy absorbers and sound absorbers or as material of hulls and shells in deep-sea applications and in aeronautics or avionics.

The porous materials such as MMSFs have increasing interest and therefore they have been more and more widely studied. The most of the papers were published about mechanical testing. Balch et al [3, 4], Dou et al [5], Kiser et al [6], Mondal et al [7], Palmer et al [8], Rabiei et al [9], Rohatgi et al [10], Tao et al [11] Wu et al [12] and Zhang et al [13] are all interested in the compressive testing of MMSFs. In the works mentioned above, the results of quasi-static, dynamic, free and constrained compression test were published in details and many parameters (like microballoon's type and size, porosity, type of matrix material etc.) were taken account. Beside this, papers on the problems of MMSF producing were also published [14–17]. Moreover Couteau and Dunand published results about the creep characteristics of MMSFs [18], while Ramachandra and Radhakrishna [19], Rohatgi et al [20] and Mondal [21] investigated the wear and corrosive properties of MMSFs. According to the wear resistance Ramachandra et al [22] and Orbulov et al [23] reported the results of various global, depth sensing, dynamic and local hardness tests.

A few papers are looking into the modelling of MMSFs or MMSF like materials. For example Bardella and Genna published two papers on the determination of the elastic properties of syntactic foams and sandwich structures consisting syntactic foams [24, 25]. These articles are based on a three phase unit

cell model considering the matrix – wall – porosity structure of the syntactic foams. Both works conclude the followings: (Eq. 1) the actual distribution of wall thickness of the microballoons seems to have little influence on the overall properties of the syntactic foams; (Eq. 2) the present of unwanted voids has a significant effect on the elastic moduli of the composite; and finally (Eq. 3) the applied three phase model gives results in good agreement with both experimental and numerical results. However according to the authors' best knowledge only polymer based syntactic foams were investigated.

Marur has done something very similar. In the first corresponding paper the author deal with the effective elastic moduli of syntactic foams [26]. An analytical approach to compute the effective elastic moduli of syntactic foams was presented. Using the three phase concentric spherical model, the effective elastic constants were estimated, and compared with other theories and experimental data. The computed effective elastic moduli were within the theoretically possible lower and upper bounds, and somewhat overestimated the experimental (polymer based) data because the supposed perfect bonding between the matrix and the microballoons. In the second paper the influence of weak interface between the inclusion and the matrix material in syntactic foam was studied using the homogenization approach [27]. The imperfect interface resulted in displacement continuity, and this displacement jump was modelled by a compliant layer with imperceptible thickness. The displacement jump at the interface was related to the corresponding traction using a linear spring model. Explicit analytical expression was derived for the homogenized bulk modulus of syntactic foam with imperfect interface. In the limit of vanishing spring layer, it reproduced bulk modulus with perfect bonding, and in the limit of vanishing tractions, it matched the bulk modulus of a porous medium. The computed effective elastic moduli were compared with experimental data available in the literature and very good agreement between the theory and test data was found.

The last four papers mentioned above deal with the elastic properties of the syntactic foams, however most of the cases also involve plastic deformation and even crack initialization and propagation. The author found only one publication on this field [28]. This is a parametric study with the determination of the crushability behaviour of conventional structural foams. Results from one-step and multistep procedures were utilized to generate the functional forms for each of the five parameters that represent various features of the stress-strain response. The functions were utilized to develop stress-strain responses of the foams at densities that were not initially available for experimental characterization. In addition, it is was also shown that the parametric forms are useful for development of "crushability maps" that can be employed for selection of a suitable-density foam for a specific application based on a certain design criterion (i.e., maximum strain-energy density or final porosity level). However the applied function would be not suitable for the modelling of MMSFs, because the sudden stress drop after the first peak in the compressive diagram.

Our aim is to develop this work further and give a mathematical description for the stress-strain curves of MMSFs. With this method any MMSF type material can be modelled and embedded into numerical programs.

2 Materials and experimental methods

The investigated materials are self-made MMSFs. The MMSFs were produced by pressure infiltration, the details were published in [23–29]. The metallic matrices were different aluminium alloys, namely Al99.5, AlSi12, AlMgSi1, AlCu5 and AlZn5 alloys. The chemical constitutions of the matrices are listed in Tab. 1.

Two kinds of microballoons (SL150 and SL300) were incorporated into the matrix materials; both of them were produced and supplied by Envirospheres Pty. Ltd. [30]. The properties of the microballoons are listed in Tab. 2 The volume fraction of the microballoons was 64 vol% in all case.

Overall ten types of MMSF blocks were produced by the combination of the different matrices and microballoons. Each block was designated by its constituents. For example $Al99.5-SL150$ means that the matrix was $Al99.55$ alloy and the reinforcement was 64 vol% of $SL150$ type microballoon. $\varnothing$ 14 mm cylindrical upsetting specimens with aspect ratio (height diameter ratio) of 1, 1.5 and 2 were machined from the produced blocks. The specimens were tested in three conditions: (i) solution treated at room temperature (sign: $ST20$), (ii) $T6$ heat treated at room temperature (sign: $HT20$) and (iii) solution treated at elevated temperature (220°C, over 0.5 homolog temperature, sign: $ST220$). For the parameters of solution and $T6$ heat treatments please see Tab. 3.

Six specimens were compressed for each condition, which means that in summary 540 upsetting tests were done (5 matrices $\times 2$ microballoon type $\times 3$ aspect ratios $\times 3$ condition $\times 6$ specimens). The engineering stress-engineering strain curves were recorded in all case and used to build up the model for their mathematical description.Origin software used to perform adequate nonlinear fittings on the recorded curves as detailed in the next section.

3 Result and discussion

The main interest of the Origin software was to permit us to approximate the stress-strain curves for various functions. The first logical way that was used was to split each curve into two parts: one part for the first peak, followed by a second part for the "plateau". We kept this method of study for each curve until the end.Here is an example of a curve hat we have approximated (see Fig. 1 for Al99.5-SL300-ST-20-1.5) The margin between the two parts is important, because at the end of the first part a crack appears in the specimen. Regarding to the first peak, our first idea was to use a Gaussian function to approximate the

Tab. 1. Chemical composition of the applied matrix materials (the significant elements are shown only)

Matrix	Main components (wt%) Al	Si	Mg	Cu	Closest ASM equivalent
Al99.5	99.5	-	-	-	Al1050
AlSi12	86	12	-	-	A413
AlMgSi1	97	1	1.2	0.3	Al6061
AlCu5	95	-	-	4.5	Al2011

Tab. 2. Morphological properties and phase constitution of the applied hollow ceramic microballoons

Type	Average diameter (μm)	Density (at 64 vol%) (g/cm^3)	Specific surface (μm^{-1})	Al_2O_3	Amorphous SiO_2	Mullite	Quartz
				wt%			
SL150	100	0.576	0.060	30-35	45-50	19	1
SL300	150	0.691	0.040				

Tab. 3. Parameters of the applied T6 heat treatments

Matrix	Solution treatment		Cooling medium	Aging	
	temperature(°C)	time (h)		temperature (°C)	time (h)
Al99.5	500	1	water	-	-
AlSi12	500	1	water	-	-
AlMgSi1	520	1	water	170	14
AlCu5	500	1	water	160	14
AlZn5	520	1	water	170	24

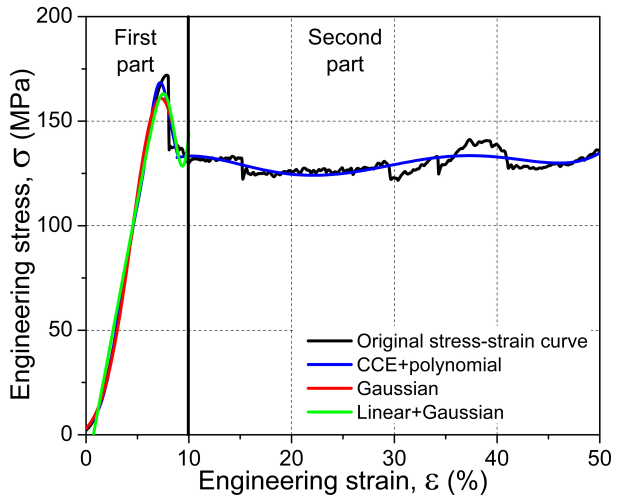

Fig. 1. Compressive stress strain curve and fitted curves of Al99.5-SL300-St-20-1.5 type MMSF

curve, while this function is ideal for modelling a simple peak.

$$y = y_0 + \frac{A}{w\sqrt{0.5\pi}} e^{-2\frac{(x-x_c)}{w^2}} \quad (1)$$

In this formulae x_c represents the abscissa of the peak, w the width of the peak, and A is used to modify the height of the peak (amplitude). However this function does not take into account the peak asymmetry. To solve this problem the next idea was to use a new function that is the sum of a Gaussian and a linear function.

$$y = y_0 + y_1 x + \frac{A}{w\sqrt{0.5\pi}} e^{-2\frac{(x-x_c)}{w^2}} \quad (2)$$

We also tried to model this first part of the curve by a double Gaussian (the sum of two Gaussians). This approximation was quite good but there were still some curves on which the approximation does not work. Therefore, after many trying and searching for asymmetrical peak functions, we opted for the Chesler-Cram Peak Function (CCE) function.

$$y = y_0 + A\left[e^{\frac{-(x-x_{c1})^2}{2w}} + B(1 - 0.5(1 - \tan h(k_2(x - x_{c2})))) \right.$$
$$\left. e^{-0.5k_3(|x-xc_3|)x-x_{c3})}\right] \quad (3)$$

where: y_0 is a sort of offset and permit to move up or down the curve, A is a multiplier that determines the peak height (amplitude), x_{c1} is the abscissa of the peak (strain at first peak), x_{c2} is the abscissa of the middle of the hyperbolic tangent which permits the asymmetry, B is the amplitude of the second exponential, w is the variance of the Gaussian part of the function (peak width), k_2 is the weight of the hyperbolic tangent, x_{c3} is the start abscissa of the second exponential, k_3 is the weight of the second exponential. The visualization of CCE curve is shown in Fig. 2.

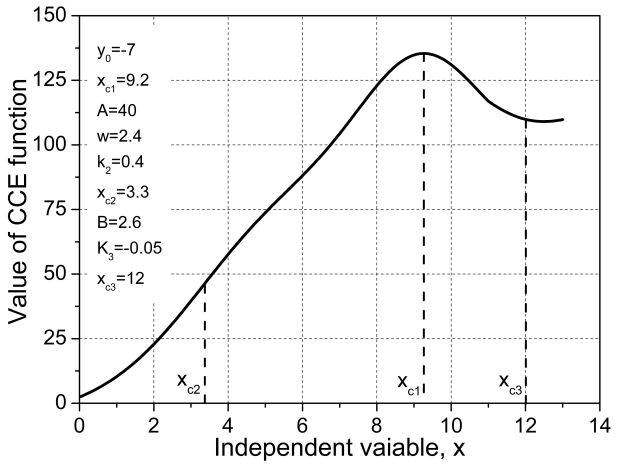

Fig. 2. The visualization of the Chesler-Cram peak function

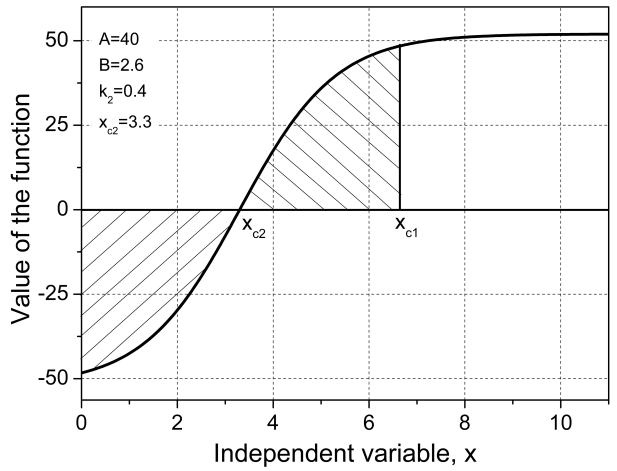

Fig. 3. Visualization for the calculation of the third integral part

For the second part of the curve, several ideas have been taken into account at the start: linear function, polynomial of second order or more, or functions like x^n. Because of the various evaluation of the second part (can increase, decrease or even alternate) an affine function or a second order polynomial can not characterize this part. Therefore a function in which the exponent is variable was the next step of our approach. However, it was not a perfect approximation. Finally fifth order polynomial was chosen. With this function we had to determine six coefficients by nonlinear fittings.

$$y = A_0 + A_1 x + A_2 x^2 + A_3 x^3 + A_4 x^4 + A_5 x^5 \qquad (4)$$

Higher order polynomials would give better fitting, but the authors stopped at fifth order because this is sufficient to describe all the variations and alternations of the curve. However the second part of the curves is only interested in energy absorption and corresponds to the failure mechanisms of MMSFs, therefore this part of the curve is not studied further in this paper, but will be detailed in our next article. In summary all the stress-strain curves of the different MMSFs can be described by using the CCE function and a fifth order polynomial. An example is shown if Fig. 1.

The first part of the curve provides the main mechanical properties of the MMSFs, namely the compressive strength (first peak), the fracture strain (strain at first peak) and the structural stiffness (the slope of the initial of the curve). Therefore the authors made a theoretical study of the CCE function (presented by (Eq. 3)) that has been useful to approximate the first part of the engineering stress – engineering strain curves.

First a simplification can be done, because the CCE is only used to describe the first part of the curves, therefore its second exponential is not necessary: due to x is always less than x_{c3}, thus

$$\forall x < x_{c3} \rightarrow e^{-0.5k_3(x-x_{c3})} + x - x_{c3} = 1 \qquad (5)$$

Therefore the original CCE function can be simplified to:

$$y = y_0 + A\left[e^{\frac{-(x-x_{c1})^2}{2w}} + B(1 - 0.5(1 - \tan h(k_2(x - x_{c2}))))\right] \qquad (6)$$

The second exponential part will be not necessary for the calculation of the compressive strength, the failure strain or the structural stiffness. The compressive strength is the value of the modified CCE function at x_{c1} and we know that for given parameters of usual MMSFs:

$$\tan h(k_2(x - x_{c2})) \approx 1 \qquad (7)$$

By combining (Eq. 6) and (Eq. 7) the compressive strength (σ_c) can be written as:

$$\sigma_c = y_0 + A(1 + B) \qquad (8)$$

The x_{c1} abscissa of the first peak, which can be obtained from the fitting, gives the failure strain (ε_c):

$$\varepsilon_c = x_{c1} \qquad (9)$$

The slope of the curve in the elastic part equals to the structural stiffness. To determine this, the slope at the point x_{c2} should be calculated by a limited development of the simplified CCE at $x = x_{c2}$. In the small vicinity of x_c2:

$$\forall x \in [x_{c2} - \delta; x_{c2} + \delta] \rightarrow e^{\frac{-(x-x_{c1})^2}{2w}} \approx 0 \qquad (10)$$

and

$$\tan h(k_2(x - x_{c2})) \approx k_2 x \qquad (11)$$

With (Eq. 10) and (Eq. 11) the structural stiffness can be expressed as:

$$S = 0.5ABk_2$$

The area under the stress – strain curve represents the energy absorbed by the material. The energy absorbed to the end of the first part is important because it represents the absorbed energy until the appearance of the first crack in the specimen. The absorbed energy equals to the integrated area below the curve and can be defined as:

$$E = \int_0^{x_{c1}} y(x)dx = I_1 + I_2 + I_3 \qquad (12)$$

where:

$$I_1 = \int_0^{x_{c1}} (y_0 + 0.5AB)dx \tag{13}$$

$$I_2 = \int_0^{x_{c1}} Ae^{\frac{-(x-x_{c1})^2}{2w}} dx \tag{14}$$

$$I_3 = \int_0^{x_{c1}} 0.5AB \tan h(k_2(x - x_{c2}))dx \tag{15}$$

The first integral is easy to calculate:

$$I_1 = (0.5AB + y_0)x_{c1} \tag{16}$$

Regarding to the second integral, as

$$\int_0^{+\infty} e^{-x^2} dx = \frac{\sqrt{\pi}}{2} \tag{17}$$

and x_{c1} is high enough compared to x_{c2}, we can approximate I_2 with a change of variable.

$$I_2 = A\sqrt{\frac{\pi w}{2}} \tag{18}$$

To calculate the third integral, the authors suggest a graphical approach. For this the plot of the function to be integrated is shown in Fig. 3.

The authors notice that the two hatched areas compensate each other; therefore their integrated value is almost zero. Due to this the third integral is the area of the rectangle between x_{c1} and x_{c2}:

$$I_3 = 0.5AB(x_{c1} - 2x_{c2}) \tag{19}$$

The authors note that certainly it is possible to calculate the exact value of the third integral by the following expression:

$$I_3 = \frac{0.5B}{k_2} \{\ln[\cosh(k_2(x_{c1} - x_{c2}))] - \ln[\cosh(-k_2 x_{c2})]\} \tag{20}$$

By summing these three integrals and rearranging the formula, we obtain a relationship linking the absorbed energy and the parameters of CCE:

$$E = y_0 x_{c1} + A\left(\sqrt{0.5\pi w} + B(x_{c1} - x_{c2})\right)$$

When all of the curves were fitted, the different parameters obtained for the modified CCE function were grouped. Thanks to the previously established formulas, we were able to trace the evolution of the compressive strength (first peak), the failure strain (strain at first peak), the structural stiffness (slope of the elastic part), and the absorbed energy (area below the curve) for a given material depending on the ratio H/D. It should be noted that some curves were not considered because the parameters obtained for the CCE function were abnormal values. Here are several examples of obtained graphs.

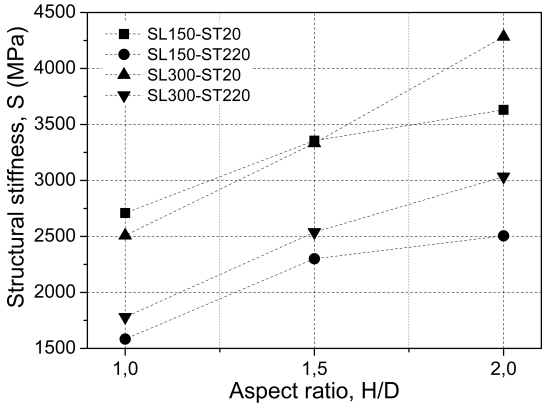

Fig. 4. Structural stiffness for different Al99.5 matrix syntactic foams

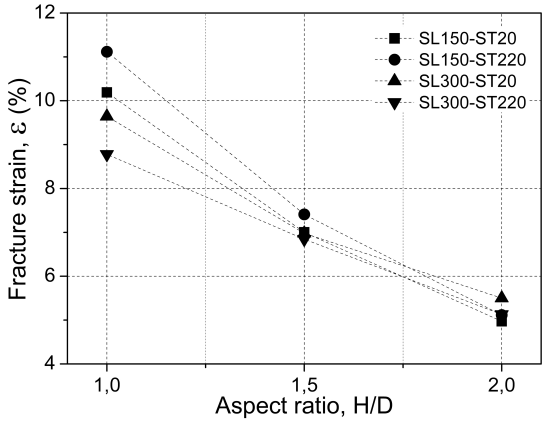

Fig. 5. Fracture strain for different Al99.5 matrix syntactic foams

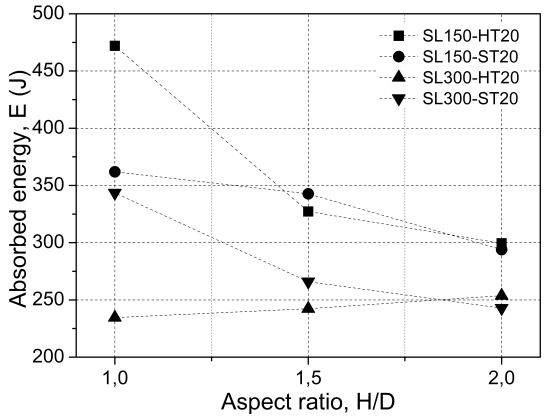

Fig. 6. Absorbed energy for different AlCu5 matrix syntactic foams

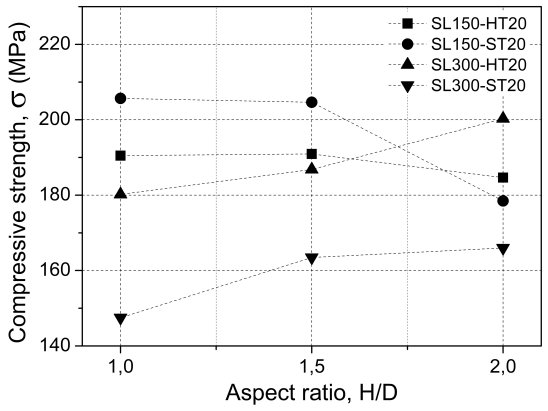

Fig. 7. Compressive strength for different AlCu5 matrix syntactic foams

The authors note that in some graphics it is easy to make conclusions. For example the graph of the slope in the quasi-elastic Al99.5 shows that the initial slope increases with H/D (Fig. 4). However, it is more difficult to make conclusions from other graphs like the graph representing the energy absorbed AlCu5 (Fig. 6). Thus, we have grouped all the trends in comparative tables for readability (please refer to Tab. 4, Tab. 5, Tab. 6, Tab. 7 in the Annex). The trends can be described as increasing, decreasing, constant, hat (with maximums around $H/D = 1.5$), valley (with minimums around $H/D = 1.5$) or "unknown" (if no general trend can be seen). In summary, some trends can be noticed: for a given material, where H/D increases, the structural stiffness (the slope of the quasi-elastic part) increases, the absorbed energy (the area below the curve) and the fracture strain decrease. Moreover, the upsetting tests conducted at 220°C lead to maximum stresses and initial slopes lower than for tests realized at 20°C. However, for some materials it is difficult to obtain convincing results. This is particularly the case of AlZn5 (especially for compressive stress). It is certain that checking all the curves, some tests could be eliminated, which would then remove some inconsistencies. It is nevertheless difficult to find the boundary between a test that can keep and one that must be eliminated.

4 Conclusions

By using the modified CCE function to describe the compressive behaviour of MMSFs, we were able to calculate the compressive strength (σ_c), the fracture strain (ε_c), the structural stiffness (S) and the absorbed energy (E) of the engineering stress – engineering strain curves. The formulas linking the physical parameters to the fitting parameters are given in the following forms:

$$\sigma_c = y_0 + A(1+B)$$
$$\varepsilon_c = x_{c1}$$
$$S = 0.5ABk_2$$
$$E = y_0 x_{c1} + A\left(\sqrt{0.5\pi\,w} + B(x_{c1} - x_{c2})\right)$$

References

1 **Babcsán N, Leitlmeier D, Banhart J**, *Metal foams–High temperature colloids Part I: Ex situ analysis of metal foams*, Coll. Surf. A:Physicochem. Eng. Asp **261** (2005), 123-130, DOI 10.1016/j.colsurfa.2004.12.030.

2 **Babcsán N, García Moreno F, Banhart J**, *Metal foams–High temperature colloids Part II: In situ analysis of metal foams*, Coll. Surf. A: Physicochem. Eng. Asp **309** (2007), 254-263, DOI doi:10.1016/j.colsurfa.2007.02.044.

3 **Balch D K, O'Dwyer J G, Davis G R, Cady C M, Gray III G T, Dunand D C**, *Plasticity and damage in aluminium syntactic foams deformed under dynamic and quasi-static conditions*, Mater. Sci. Eng. A **391** (2005), 408-417, DOI doi:10.1016/j.msea.2004.09.012.

4 **Balch D K, Dunand D C**, *Load partitioning in aluminum syntactic foams containing ceramic microspheres*, Acta Mater. **54** (2006), 1501-1511, DOI 10.1016/j.actamat.2005.11.017.

5 **Dou Z Y, Jiang L T, Wu G H, Zhang Q, Xiu Z Y**, *High strain rate compression of cenosphere-pure aluminium syntactic foams*, Scripta Mater **57** (2007), 945-948, DOI 10.1016/.j.scriptamat.2007.07.024.

6 **Kiser M, He M Y, Zok F W**, *The mechanical response of ceramic microballoon reinforced aluminum matrix composites under compressive loading*, Acta Mater **47** (1999:9), 2685-2694.

7 **Mondal D P, Das S, Ramakrishnan N, Uday Bhasker K**, *Cenosphere filled aluminium syntactic foam made through stir-casting technique*, Compos. Part A **40** (2009), 279-288, DOI 10.1016/j.compositesa.2008.12.006.

8 **Palmer R A, Gao K, Doan T M, Green L, Cavallaro G**, *Pressure infiltrated syntactic foams – Process development and mechanical properties*, Mater. Sci. Eng.A **464** (2007), 85-92.

9 **Rabiei A, O'Neill A T**, *A study on processing of a composite metal foam via casting*, Mater. Sci. Eng. A **404** (2005), 159-164.

10 **Rohatgi P K, Kim J K, Gupta N, Alaraj S, Daoud A**, *Compressive characteristics of A356/fly ash cenosphere composites synthesized by pressure infiltration technique*, Compos. Part A **37** (2006), 430-437.

11 **Tao X F, Zhao Y Y**, *Compressive behaviour of Al matrix syntactic foams toughened with Al particles*, Scripta Mater **61** (2009), 461-464, DOI 10.1016/j.scriptamat.2009.04.045.

12 **Wu G H, Dou Z Y, Sun D L, Jiang L T, Ding B S, He B F**, *Compression behaviours of cenosphere-pure aluminium syntactic foams*, Scripta Mater.C **56** (2007), 221-224.

13 **Zhang L P, Zhao Y Y**, *Mechanical response of Al matrix syntactic foams produced by pressure infiltration casting*, J. Compos. Mater **41** (2007), 2105-2117.

14 **Bárczy T, Kaptay G.**, *Modeling the infiltration of liquid metals into porous ceramics*, Mater. Sci. Forum **14** (2005), 473-474.

15 **Trumble P K**, *Spontaneous infiltration of non-cylindrical porosity: close-packed spheres*, Acta Mater **46** (1998), 2363-2367.

16 **Rohatgi P K, Guo R Q, Iksan H, Borchelt E J, Asthana R**, *Pressure infiltration technique for synthesis of aluminium-fly ash particulate composite*, Mater. Sci. Tech. A **244** (1998), 22-30.

17 **Orbulov I N**, *Syntactic foams produced by pressure infiltration – the effect of pressure and time on infiltration length*, Per. Pol. Mech. Eng. **2010/2** (2010), DOI 10.3311/ppme.2010-2.05.

18 **Couteau O, Duanand D C**, *Creep of aluminium syntactic foams*, Mater. Sci. Eng. A **488** (2008), 573-579, DOI 10.1016/j.msea.2008.01.022.

19 **Ramachandra M, Radhakrishna K**, *Effect of reinforcement of flyash on sliding wear, slurry erosive wear and corrosive behaviour of aluminium matrix composite* **Wear** (2007), no. 262, 1450-1462.

20 **Rohatgi P K, Guo P K**, *Mechanism of abrasive wear of Al-Si hypoeutectic alloy containing 5 vol% fly ash*, Tribol. Let **3** (1997), 339-347.

21 **Mondal D P, Das J, Jha N**, *Dry sliding wear behaviour of aluminium syntactic foam*, Mater. Des **30** (2008), 2563-2568.

22 **Ramachandra M, Radhakrishna K**, *Synthesis-microstructure-mechanical properties-wear and corrosion behaviour of an Al-Si (12%)-Flyash metal matrix composite*, J. Mater. Sci. **40** (2005), 5989-5997.

23 **Orbulov I N, Németh Á**, *Global, depth sensing and dynamic hardness of metal matrix syntactic foams*, Per. Pol. Mech. Eng **53** (2009:2), 93-99, DOI 0.3311/pp.me.2009-2.07.

24 **Bardella L, Genna F**, *On the elastic behaviour of syntactic foams*, Int. J. Sol. Struc **38** (2001), 7235-7260.

25 **Bardella L., Genna F**, *Elastic design of syntactic foamed sandwiches obtained by filling of three-dimensional sandwich-fabric panels*, Int. J. Sol. Struc. **38** (2001), 307-333.

26 **Marur P R**, *Effective elastic moduli of syntactic foams*, Mater. Let. **59** (2005), 1954-1957, DOI 10.1016/j.matlet.2005.02.034.

27 **Marur P R.**, *Influence of imperfect interface on the elastic moduli of syntactic foams*, Comp. Mater. Sci. **46** (2009), 327-332, DOI 10.1016/j.commatsci.2009.03.010.

28 **Liu Q, Subhash G, Gao X-L**, *A parametric study on crushability of open-cell structural polymeric foams*, J. Por. Mater **12** (2005), 233-248.
29 **Orbulov I N, Dobránszky J**, *Producing metal matrix syntactic foams by pressure infiltration*, Per. Pol. Mech. Eng. **52** (2008:1), 1-8.
30 **Envirospheres Pty. Ltd.**, 30^{th} June 2011., available at `www.envirospheres.com`.

Tab. 4. Trend of the compressive strenght in function of aspect ratio

Matrix	Microballon's type	Condition	Trend as the function of aspect ratio	Notes
Al99.5	SL150	ST 20	decrease	ST 220<ST 20 SL150=SL300 except H/D=2, when SL300>SL150
		ST 220	decrease	
	SL300	ST 20	decrease	
		ST 220	decrease	
AlSi12	SL150	ST 20	decrease	ST 220<ST 20
		ST 220	unknown	
	SL300	ST 20	decrease	
		ST 220	constant	
AlMgSi1	SL150	ST 20	constant	SL300<SL150
		HT 20	constant	
	SL300	ST 20	constant	
		HT 20	constant	
AlCu5	SL150	ST 20	increase	
		HT 20	hat	
	SL300	ST 20	valley	
		HT 20	hat	
AlZn5	SL150	ST 20	constant	HT 20>ST 20
		HT 20	unknown	
	SL300	ST 20	unknown	
		HT 20	unknown	

Tab. 5. Trend of the fracture strain in function of aspect ratio

Matrix	Microballon's type	Condition	Trend as the function of aspect ratio	Notes
Al99.5	SL150	ST 20	decrease	
		ST 220	decrease	
	SL300	ST 20	decrease	
		ST 220	decrease	
AlSi12	SL150	ST 20	decrease	
		ST 220	unknown	
	SL300	ST 20	decrease	
		ST 220	decrease	
AlMgSi1	SL150	ST 20	decrease	HT20>ST20 SL150>SL300
		HT 20	decrease	
	SL300	ST 20	decrease	
		HT 20	decrease	
AlCu5	SL150	ST 20	decrease	
		HT 20	decrease	
	SL300	ST 20	decrease	
		HT 20	decrease	
AlZn5	SL150	ST 20	decrease	SL150>SL300 HT20>ST20
		HT 20	decrease	
	SL300	ST 20	decrease	
		HT 20	decrease	

Tab. 6. Trend of the structural stiffness in function of aspect ratio

Matrix	Microballon's type	Condition	Trend as the function of aspect ratio	Notes
Al99.5	SL150	ST 20	increase	ST20>ST220 SL150=SL300 except HD2 SL300>SL150
		ST 220	increase	
	SL300	ST 20	increase	
		ST 220	increase	
AlSi12	SL150	ST 20	increase	
		ST 220	unknown	
	SL300	ST 20	increase	
		ST 220	increase	
AlMgSi1	SL150	ST 20	increase	
		HT 20	hat	
	SL300	ST 20	increase	
		HT 20	unknown	
AlCu5	SL150	ST 20	increase	
		HT 20	increase	
	SL300	ST 20	increase	
		HT 20	increase	
AlZn5	SL150	ST 20	increase	HT 20<ST 20
		HT 20	increase	
	SL300	ST 20	increase	
		HT 20	increase	

Tab. 7. Trend of the absorbed energy in function of aspect ratio

Matrix	Microballon's type	Condition	Trend as the function of aspect ratio	Notes
Al99.5	SL150	ST 20	decrease	SL150=SL300 except HD2 SL300>SL150
		ST 220	decrease	
	SL300	ST 20	decrease	
		ST 220	decrease	
AlSi12	SL150	ST 20	decrease	ST220<ST20
		ST 220	unknown	
	SL300	ST 20	decrease	
		ST 220	decrease	
AlMgSi1	SL150	ST 20	decrease	
		HT 20	valley	
	SL300	ST 20	decrease	
		HT 20	decrease	
AlCu5	SL150	ST 20	decrease	SL300<SL150
		HT 20	decrease	
	SL300	ST 20	decrease	
		HT 20	constant	
AlZn5	SL150	ST 20	constant	
		HT 20	decrease	
	SL300	ST 20	decrease	
		HT 20	decrease	